# Elastic, diffusion, and viscosity cross sections for collisions involving excited atomic hydrogen

R. Celiberto,[1,3] U. T. Lamanna,[2,3] and M. Capitelli[1,3]
[1]*Centro di Studio per la Chimica dei Plasmi del CNR, Bari, Italy*
[2]*Centro Studi Chimico-Fisici sull'interazione luce-materia del CNR, Bari, Italy*
[3]*Dipartimento di Chimica, Universita' di Bari, Bari, Italy*
(Received 16 October 1997; revised manuscript received 1 May 1998)

Elastic, diffusion, and viscosity cross sections for collisions of two hydrogen atoms in excited electronic states have been calculated by solving the Schrödinger equation with interaction potentials obtained by full configuration-interaction calculations. Viscosity and thermal conductivity have been reported as a function of the principal quantum number. [S1050-2947(98)06009-0]

PACS number(s): 34.50.−s, 34.10.+x, 52.20.Hv, 52.25.Fi

## I. INTRODUCTION

The recent studies on fusion edge plasmas and divertor plasmas, connected with the ITER (International Thermonuclear Experimental Reactor) project, have placed new emphasis on atomic and molecular processes involving H and D species. Actually, the relatively low electron temperatures achieved in these systems allow for the formation of high-density neutral species, which play a crucial role in determining the plasma properties [1].

In this frame a renewed interest [2] has been recently devoted to the calculation of elastic and transport cross sections of atomic hydrogen, due to their importance in the cooling of plasmas before its impact with the reactor wall. This kind of interest, however, has been limited to hydrogen atoms in their ground state. On the other hand, construction of accurate collisional-radiative models for atomic hydrogen, as well as accurate determinations of transport coefficients of plasmas, needs the knowledge of transport cross sections of atomic hydrogen in electronically excited states as well as accurate determinations of the transport coefficients of plasmas. Surprisingly, still today the only knowledge of transport cross sections of excited atomic hydrogen is that discussed many years ago by some of the present authors [3,4]. These papers in particular deal with the collision integrals of the $H(n)$-$H(1s)$ and $H(n)$-$H^+$ interactions where $H(n)$ denotes a hydrogen atom with principal quantum number $n$. Transport cross sections for the $H(n)$-$H(n)$ interaction was in contrast limited to $n=2$ due to the then poor knowledge of potential curves arising in the interaction of excited atomic hydrogen. Since then, quantum chemistry provided us accurate sets of potential curves arising in this kind of interaction so that we can now use them for obtaining information about the corresponding transport properties.

In this paper, we report elastic and transport (diffusion and viscosity) cross sections for the scattering system $H(n)+H(n)$, with $n=1,2,3,4,5$. The interaction potentials, which have been obtained by performing full configuration-interaction (CI) calculations, are restricted only to some specific singlet states that, as discussed below, can be considered representative of the entire manifold, leaving to a future work a complete characterization of the excited states of the $H_2$ molecule.

## II. METHOD OF CALCULATION AND NUMERICAL DETAILS

The Schrödinger equation for two hydrogen atoms, colliding in the center-of-mass coordinate system, can be written as [5]

$$\left(\hat{H}_M-\frac{\hbar^2}{2\mu}\nabla_R^2-E\right)\Psi(r_i,s_i,s_n,\vec{R})=0, \tag{1}$$

where $r_i$, $s_i$, and $s_n$ represent collectively the position vectors of the electrons and the electron and nuclear spin coordinates, respectively. $\vec{R}$ is the internuclear distance vector and $\mu$ is the nuclei reduced mass. $\hat{H}_M$ is the Hamiltonian for the molecular system defining the eigenfunctions $\Phi_\Gamma(r_i,s_i;R)$ for the $\Gamma$ electronic state as

$$\hat{H}_M\Phi_\Gamma(r_i,s_i;R)=E_\Gamma(R)\Phi_\Gamma(r_i,s_i;R). \tag{2}$$

Expanding now the total scattering wave function in molecular states as [5]

$$\Psi(r_i,s_i,s_n,\vec{R})=\sum_\Gamma F_\Gamma(\vec{R},s_n)\Phi_\Gamma(r_i,s_i;R) \tag{3}$$

and inserting this expression in Eq. (1), we obtain a set of $\Gamma$ equations of the form

$$\left[-\frac{\hbar^2}{2\mu}\nabla_R^2-E_\Gamma(R)-E\right]F_\Gamma(\vec{R},s_n)=0, \tag{4}$$

where the coupling terms have been neglected (adiabatic approximation [5]).

For slow collisions, we may assume for the total wave function $\Psi$ the simple form

$$\Psi(r_i,s_i,s_n,\vec{R})\approx F_\Gamma(\vec{R},s_n)\Phi_\Gamma(r_i,s_i;R), \tag{5}$$

which establishes that the scattering process is governed by the potential interaction energy corresponding to the molecular state described by the wave function $\Phi_\Gamma(r_i,s_i;R)$.

Imposing the appropriate asymptotic conditions, and taking into account the nuclear symmetry [5], the final expression for the elastic cross sections is written as

 

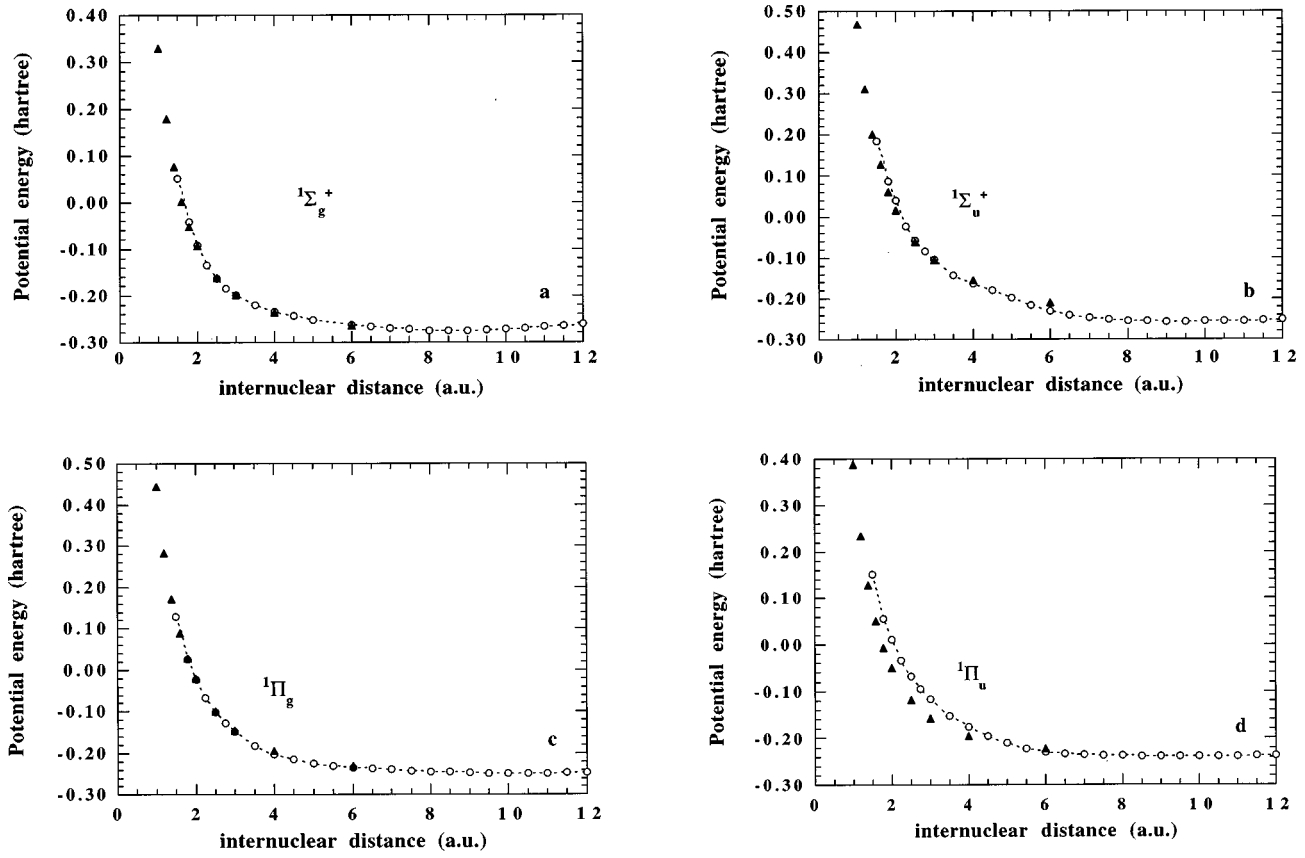


FIG. 1. (a)–(d) Potential energies of some electronic states arising in the singlet interaction of two excited ($n=2$) hydrogen atoms. Circles, present results; triangles, Ref. [10].

$$\sigma_e(E)=\frac{8\pi}{k^2}\left[\tfrac{1}{4}\sum_{l(\text{even})}^{\infty}(2l+1)\sin^2\delta_l^{\Gamma}+\tfrac{3}{4}\sum_{l(\text{odd})}^{\infty}(2l+1)\sin^2\delta_l^{\Gamma}\right], \tag{6}$$

where $E$ is the collision energy and $k$ is given by

$$k^2=\frac{2\mu E}{\hbar^2}, \tag{7}$$

$\delta_l^{\Gamma}$ represents the $l$th phase shift, while the statistical weights 1/3 and 3/4 refer to the nuclear spin states.

Similar expressions can be obtained for diffusion and viscosity cross sections [6]:

$$\sigma_D=\frac{8\pi}{k^2}\left[\tfrac{1}{4}\sum_{l(\text{even})}^{\infty}(l+1)\sin^2(\delta_{l+1}^{\Gamma}-\delta_l^{\Gamma})+\tfrac{3}{4}\sum_{l(\text{odd})}^{\infty}(l+1)\sin^2(\delta_{l+1}^{\Gamma}-\delta_l^{\Gamma})\right], \tag{8}$$

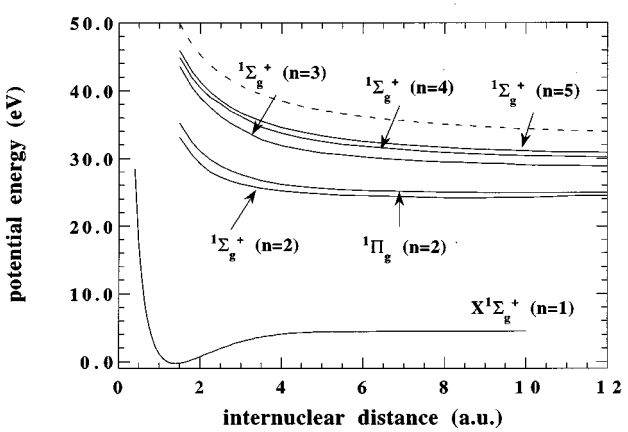


FIG. 2. Potential-energy curves for the singlet electronic states relative to the H($n$)-H($n$) interaction. Solid lines: $n=1,2,3,4,5$; dashed line: electron-electron Coulomb potential.

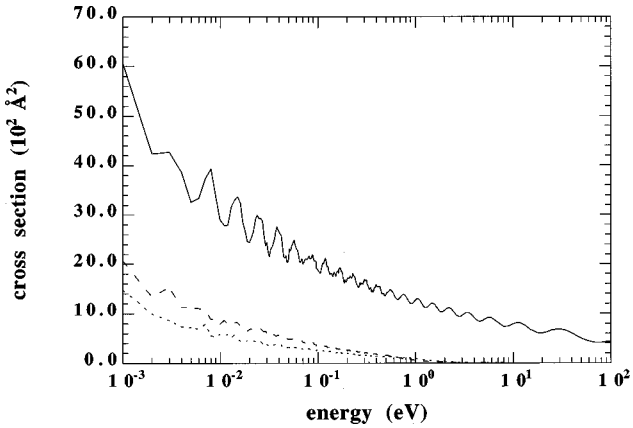


FIG. 3. Elastic (solid line), diffusion (dashed line), and viscosity (dotted line) cross sections for the H($n=2$)+H($n=2$) $^1\Sigma_g^+$ interaction.

TABLE I. Interaction potential energies (Hartree) as a function of the internuclear distance $R$ (a.u.)for the system $H(n)+H(n)$ with $n=2,3,4,5$.

| $R$ | $^1\Sigma_g^+$ $(n=2)$ | $^1\Pi_g$ $(n=2)$ | $^1\Sigma_g^+$ $(n=3)$ | $^1\Sigma_g^+$ $(n=4)$ | $^1\Sigma_g^+$ $(n=5)$ |
|---|---|---|---|---|---|
| 1.50 | 0.051377 | 0.12958 | 0.43701 | 0.48673 | 0.52172 |
| 1.80 | −0.040963 | 0.026247 | 0.32402 | 0.37611 | 0.41018 |
| 2.00 | −0.091637 | −0.021890 | 0.26878 | 0.32086 | 0.35371 |
| 2.25 | −0.13505 | −0.067173 | 0.21590 | 0.27111 | 0.29787 |
| 2.50 | −0.16326 | −0.10120 | 0.16778 | 0.23454 | 0.25424 |
| 2.75 | −0.18400 | −0.12739 | 0.12958 | 0.19644 | 0.21727 |
| 3.00 | −0.19974 | −0.14795 | 0.098545 | 0.16771 | 0.18523 |
| 3.50 | −0.22317 | −0.18195 | 0.041514 | 0.10947 | 0.14120 |
| 4.00 | −0.23795 | −0.20206 | 0.0072505 | 0.076499 | 0.10611 |
| 4.50 | −0.24788 | −0.21528 | −0.014054 | 0.050667 | 0.082340 |
| 5.00 | −0.25520 | −0.22415 | −0.031890 | 0.030635 | 0.062645 |
| 5.50 | −0.26078 | −0.23019 | −0.041911 | 0.016105 | 0.046661 |
| 6.00 | −0.26469 | −0.23439 | −0.052434 | 0.0049806 | 0.032829 |
| 6.50 | −0.26721 | −0.23742 | −0.062325 | −0.0043062 | 0.022207 |
| 7.00 | −0.26968 | −0.23979 | −0.069978 | −0.014119 | 0.012933 |
| 7.50 | −0.27265 | −0.24190 | −0.076717 | −0.022667 | 0.0046005 |
| 8.00 | −0.27514 | −0.24395 | −0.081082 | −0.028670 | −0.0019799 |
| 8.50 | −0.27624 | −0.24576 | −0.084112 | −0.034768 | −0.0079314 |
| 9.00 | −0.27590 | −0.24711 | −0.087292 | −0.040174 | −0.012881 |
| 9.50 | −0.27447 | −0.24796 | −0.091758 | −0.044502 | −0.015396 |
| 10.0 | −0.27235 | −0.24839 | −0.096433 | −0.046894 | −0.020391 |
| 10.5 | −0.26986 | −0.24847 | −0.099114 | −0.048725 | −0.023885 |
| 11.0 | −0.26724 | −0.24829 | −0.10030 | −0.050201 | −0.026212 |
| 11.5 | −0.26461 | −0.24790 | −0.10113 | −0.052258 | −0.028415 |
| 12.0 | −0.26208 | −0.24736 | −0.10594 | −0.054899 | −0.031682 |

$$\sigma_\eta=\frac{8\pi}{k^2}\left[\tfrac{1}{4}\sum_{l(\text{even})}^{\infty}\frac{(l+1)(l+2)}{(2l+3)}\sin^2(\delta_{l+2}^{\Gamma}-\delta_l^{\Gamma})+\tfrac{3}{4}\sum_{l(\text{odd})}^{\infty}\frac{(l+1)(l+2)}{(2l+3)}\sin^2(\delta_{l+2}^{\Gamma}-\delta_l^{\Gamma})\right]. \quad (9)$$

The scattering of two electronically excited hydrogen atoms can occur, in an adiabatic collision, through the potential interactions corresponding to a number of molecular states [7], which arise during the collision process, and correlating to a given quantum state of the free atoms. In this case, the global cross section is evaluated by performing a weighted sum of the individual cross sections obtained by using in Eq. (4) the $E_\Gamma(R)$ interaction potential associated to any distinct molecular state [3,5]. In the present paper, however, we have selected only a few singlet electronic states, correlating with the free H atoms with a given $n$ value. In particular for $n=2$, the elastic and transport cross sections have been calculated for the $^1\Sigma_g^+$ and $^1\Pi_u$ molecular interactions, to which has been attributed in the global cross section, the statistical weights of 1/3 and 2/3, respectively, while for the other $^1\Sigma_g^+$ states, corresponding to $n=3,4,5$ the statistical weight has been assumed to be unity.

The phase shifts, for a given $E_\Gamma(R)$ potential, have been calculated by solving the Schrödinger equation by the standard Numerov method. The code has been checked by reproducing the Gersh and Bernstein singlet and triplet elastic

TABLE II. Fitting coefficients for the potential curves (see text): $C_6$ (hartree bohr$^6$), $C_8$ (hartree bohr$^8$), $A_n$ (hartree bohr), and $B_n$ (bohr$^{-1}$). Numbers in square brackets denote the power of 10 factors.

| | $C_6$ | $C_8$ | $A_n$ | $B_n$ |
|---|---|---|---|---|
| $^1\Sigma_g^+$ $(n=2)$ | −6.8571[+4] | 4.6209[+6] | 1.3801 | 0.73754 |
| $^1\Pi_g$ $(n=2)$ | | | 1.0659 | 0.42117 |
| $^1\Sigma_g^+$ $(n=3)$ | | | 1.1195 | 0.19757 |
| $^1\Sigma_g^+$ $(n=4)$ | | | 1.0673 | 0.16180 |
| $^1\Sigma_g^+$ $(n=5)$ | | | 1.0656 | 0.16171 |

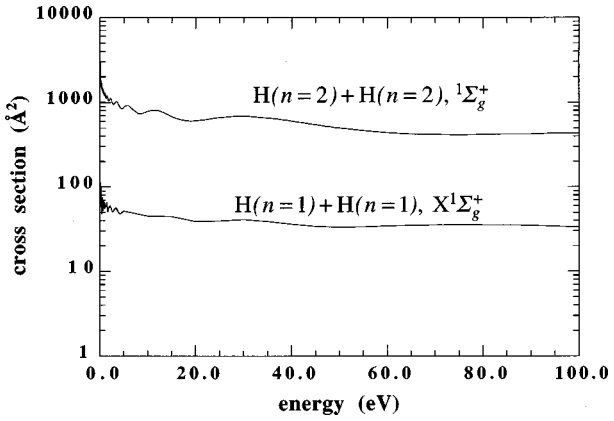


FIG. 4. Elastic cross section for $H(n=1)+H(n=1)$ $X\ ^1\Sigma_g^+$ interaction, and $H(n=2)+H(n=2)$ $^1\Sigma_g^+$ interaction.

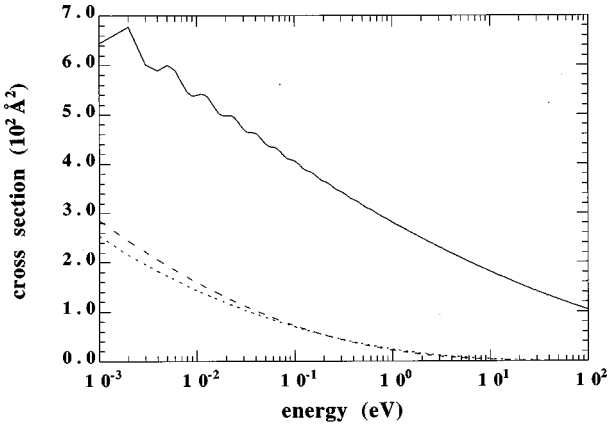


FIG. 5. Same as Fig. 3 for H($n=2$)+H($n=2$) $^1\Pi_g$ interaction.

cross sections [8] for the case H($1s$)+H($1s$), by using the interaction potentials given by Kolos and Wolniewicz [9].

For $n>1$, the electronic potentials for singlet states have been obtained by performing full CI calculations by using three different basis sets of STO orbitals. 43 STO functions were used in the range of $R<2$ a.u., 49 STO functions in the range $2<R<3$ a.u., and 55 STO functions for $R>3$ a.u. The basis included *s*, *p*, and *d* STO orbitals. In the full CI calculations all the single and double excitations were considered.

The potential curves for the $^1\Sigma_g^+$ and $^1\Pi_u$ states, correlating with the free atoms H($n=2$)+H($n=2$), are compared in Figs. 1(a)–1(d) with those reported by Guberman [10]. A good agreement is found between the two sets of results, except for the $^1\Pi_u$ states in Fig. 1(d), where some discrepancy is observed for internuclear distances $<4$ a.u. No data are available, to our knowledge, for the potential-energy curves correlating with atomic states defined by $n>2$.

The cross sections have been calculated by utilizing some of those potential curves converging at large internuclear distance to the asymptotic energy of $-1/n^2$ (hartrees). The selected potentials for $n=2,3,4,5$ are shown in Fig. 2, while the numerical data are reported in Table I. In the same figure is shown also, as a comparison, the interaction potential for two 1*s* hydrogen atoms corresponding to the molecular state $X\ ^1\Sigma_g^+$ [9].

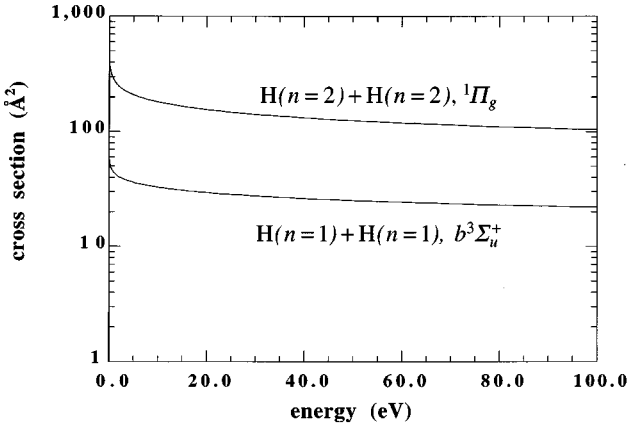


FIG. 6. Elastic cross section for H($n=1$)+H($n=1$) $b\ ^1\Sigma_u^+$ interaction [8], and H($n=2$)+H($n=2$) $^1\Pi_g$ interaction (present results).

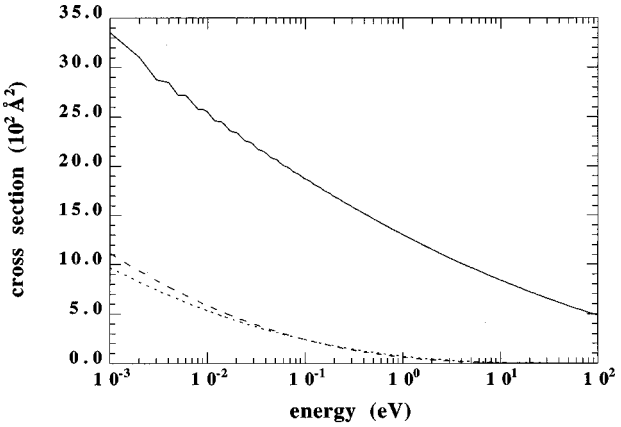


FIG. 7. Same as Fig. 3 for H($n=3$)+H($n=3$) $^1\Sigma_g^+$ interaction.

The potential values entering in the integration of the Schrödinger equation have been obtained by linear interpolation of the computed data or, in the asymptotic regions, by extrapolating the available data using somewhat standard expressions. For the state $^1\Sigma_g^+$ ($n=2$) of Fig. 2, which presents an attractive potential, we used for large $R$ the following expression:

$$V(R)=-C_6/R^6-C_8/R^8-1/n^2, \tag{10}$$

where $R$ is the internuclear distance and the constants $C_6$ and $C_8$ have been evaluated by performing a fitting procedure of the data of Table I in the range $10\leqslant R\leqslant 12$ (a.u.). For $R<1.5$ (a.u.), we assumed for the repulsive part of the $^1\Sigma_g^+$ ($n=2$) potential the usual exponential form:

$$V(R)=A_n\exp(-B_nR)/R-1/n^2, \tag{11}$$

where the $A_n$ and $B_n$ coefficients were obtained once again by fitting the data of Table I in the range $1.5\leqslant R\leqslant 3.5$ (a.u.).

Finally, the expression in Eq. (11) has been also adopted to fit all the other repulsive potential curves used in the cross-section calculations. The fitting coefficients $C_6$, $C_8$, $A_n$, and $B_n$ for all the potential functions are reported in Table II.

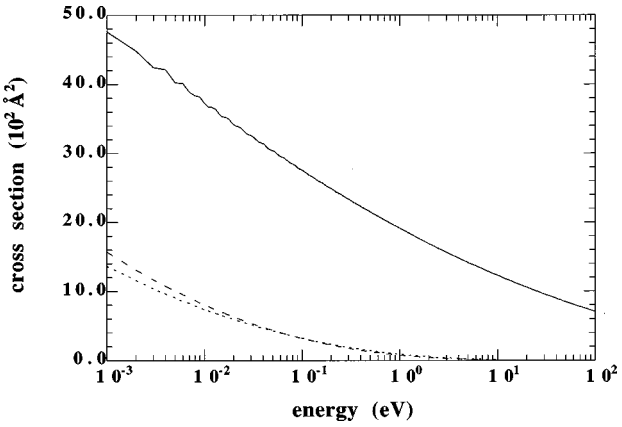


FIG. 8. Same as Fig. 3 for H($n=4$)+H($n=4$) $^1\Sigma_g^+$ interaction.

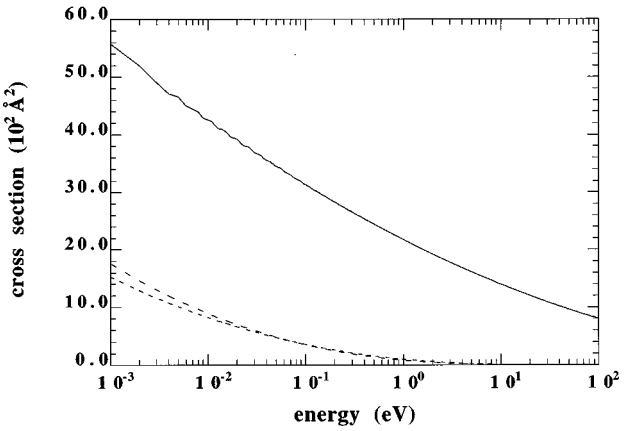


FIG. 9. Same as Fig. 3 for H($n=5$)+H($n=5$) $^1\Sigma_g^+$ interaction.

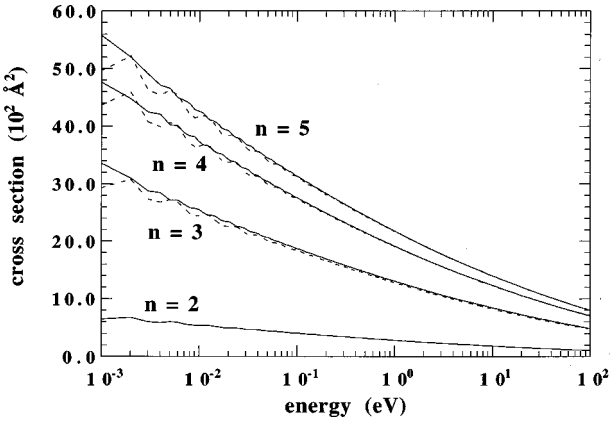


FIG. 10. Comparison between calculated (solid lines) and scaled (dashed lines) elastic cross sections [Eq. (13)] for H($n$)+H($n$) interactions.

## III. RESULTS

In Fig. 3, the elastic and transport (viscosity and diffusion) cross sections for the system H($n=2$)+H($n=2$) are shown as a function of the collision energy in the range between 0.001 and 100 eV. The corresponding $^1\Sigma_g^+$ ($n=2$) interaction potential (see Fig. 2) exhibits a minimum placed at $R\approx 8.5$ a.u.. The attractive well presents a zero-point energy of $\approx$0.7 eV below the dissociation energy. A comparison of the $n=2$ elastic cross section (see Fig. 4), with those for the singlet potential $X\ ^1\Sigma_g^+$ of two 1$s$ hydrogen atoms [9], which presents a very deep well located at smaller internuclear distances, shows that these last cross sections are significantly lower than those for the excited state [11] (more than a factor of 10). This is probably due to the fact that the elastic cross section, as it is well known, is greatly affected by the long-range forces, which, in the case of excited atoms, vanish at larger internuclear separations with respect to the $X\ ^1\Sigma_g^+$ potential (Fig. 2).

The diffusion and viscosity cross sections, also plotted in Fig. 3, lie well below the elastic one. The two curves show very close values and practically overlap for high energies.

In Fig. 5 the cross sections are reported for the case H($n=2$)+H($n=2$) interacting through the $^1\Pi_g$ state, characterized by a completely repulsive potential curve. The elastic and transport cross sections present a smooth dependence on the collision energy and quite lower values with respect to the previous case. This last feature can be attributed to the completely repulsive nature of the interaction potential.

In Fig. 6, the cross sections for the $^1\Pi_g$ state are reported for comparison along with those relative to the repulsive triplet state $b\ ^3\Sigma_u^+$ correlating to the free atoms H(1$s$) +H(1$s$) [9,11]. Again we observe an increase up to a factor of 10 in the elastic cross sections passing from the $b\ ^3\Sigma_u^+$ to the $^1\Pi_g$ state, while both the cross sections show the same dependence on the collision energy.

Elastic cross sections for $n=3,4,5$ ($^1\Sigma_g^+$) are shown in Figs. 7, 8, and 9, respectively (solid lines). Inspection of these figures shows that the $^1\Sigma_g^+$ repulsive potentials determine a behavior very similar to the one observed in Fig. 5, although the values of the cross sections increase with increasing the principal quantum number $n$. This last point can be better appreciated in Fig. 10, where we report the elastic cross sections (solid lines) as a function of incident energy for $n=2$ ($^1\Pi_g$) and $n>2$ ($^1\Sigma_g^+$).

The regular enhancement of the curves can be reproduced by an approximated scaling law. The high-energy Born cross section $\sigma_n(E)$, for a repulsive potential [Eq. (11)], is given by [12]

$$\sigma_n(E)\approx \frac{4\pi A_n^2}{B_n^2 4k^2}. \tag{12}$$

Assuming $A_n\approx 1$ (see Table II), the scaling law for elastic cross sections can be written as

$$\sigma_n(E)\approx \frac{B_{n=2}^2}{B_n^2}\,\sigma_{n=2}(E). \tag{13}$$

The scaled cross sections obtained from Eq. (13) are also shown in Fig. 10 (dashed lines). For higher energies the agreement with the exact results is particularly good, while at low energies ($<10^{-2}$ eV), the scaled cross sections reproduce the same structures of the $n=2$ curve.

The coefficients $B_n$ in Eq. (11) can be interpreted as the inverse of the screening constant in the Coulomb interaction of two hydrogen atoms [13]. This means that as the principal quantum number increases, increase the dimensions of the two atoms, so that the screening constant becomes infinitely large and the expression in Eq. (11) reduces asymptotically to a purely Coulomb potential. This can be better appreciated in Fig. 2, where the potential curves seem to converge, for high $n$, to the curve representing the electron-electron Coulomb interaction (dashed line). This is confirmed also by the scaling law in Eq. (13), which shows that the cross section asymptotically diverges as a function of $n$, due to the fact that $B_n$ decreases for high $n$ values (see Table II), reproducing the expected cross-section behavior for a Coulomb interaction.

In Figs. 7–9 the transport cross sections are also shown (dashed and dotted lines) for the case $n>3$. This cross sections have been found in excellent agreement with the classical results reported by Hong-sup Hahn *et al.* [13], who used in their calculations a screened Coulomb potential.

TABLE III. $\Omega^{*(2,2)}_{\mathrm{H}(1s)\text{-}\mathrm{H}(1s)}(T)[r_m^2\ (\text{Å}^2)]$ for singlet ($X\ ^1\Sigma_g^+$) and triplet ($b\ ^3\Sigma_u^+$) H($1s$)-H($1s$) interactions, respectively, as a function of the temperature.

| $T$ ($10^3$ K) | singlet | triplet | total | Ref. [3] |
|---|---|---|---|---|
| 10 | 1.15 | 1.81 | 2.96 | 2.60 |
| 12 | 1.03 | 1.63 | 2.66 | 2.42 |
| 14 | 0.919 | 1.49 | 2.41 | 2.25 |
| 16 | 0.823 | 1.37 | 2.19 | 2.09 |
| 18 | 0.739 | 1.27 | 2.01 | 1.96 |
| 20 | 0.665 | 1.18 | 1.85 | 1.84 |
| 25 | 0.521 | 1.00 | 1.52 | 1.59 |

## IV. TRANSPORT PROPERTIES

### A. Collision integrals

In order to check the present calculations for the plasma transport properties, we have compared the quantity

$$\Omega^{*(2,2)}_{\mathbf{H}(n)-\mathrm{H}(n)}(T)r_m^2=\frac{\overline{\sigma_\eta(T)}}{4\pi} \tag{14}$$

with the results reported by Capitelli and Lamanna [3] for $n=1$ and $n=2$ cases. $\Omega^{*(2,2)}_{\mathrm{H}(n)\text{-}\mathrm{H}(n)}(T)$ in the above equation is the collision integral depending on the absolute temperature $T$ and relative to the H($n$)-H($n$) interaction, while $r_m$ is the collision diameter [14]. $\overline{\sigma_\eta(T)}$ is the viscosity cross section averaged over a Maxwellian distribution by using the expression [15]

$$\overline{\sigma_\eta(T)}=\frac{1}{(kT)^4}\int_0^\infty E^3 e^{-E/kT}\sigma_\eta(E)dE, \tag{15}$$

where $k$ represents the Boltzmann constant.

For $n=1$, the collision integral $\Omega^{*(2,2)}_{\mathrm{H}(1s)\text{-}\mathrm{H}(1s)}(T)r_m^2$, evaluated in this case by including in the $\sigma_\eta(E)$ also the triplet contribution, has been successfully compared with the Capitelli-Lamanna results (see Table III).

A good agreement has been found also for $\Omega^{*(2,2)}_{\mathrm{H}(n=2)\text{-}\mathrm{H}(n=2)}(T)r_m^2$. This last case is shown in Fig. 11, where $\Omega^{*(2,2)}_{\mathrm{H}(n=2)\text{-}\mathrm{H}(n=2)}(T)r_m^2$, obtained by performing a weighted sum of the two contributions coming from the $^1\Sigma_g^+$ and $^1\Pi_g$ interactions, is compared with the results taken from Ref. [3], as a function of the absolute temperature. The dependence of the Capitelli-Lamanna cross sections on the absolute temperature is well reproduced by the present results, even though a factor $\approx 1.5$ separates the two curves. This difference could be ascribed to the lack, in our calculations, of the contribution coming from other singlet and triplet states correlating with the free H($n=2$) atoms, as it is suggested by the cross sections relative to the $^1\Sigma_g^+$ and $^1\Pi_g$ interactions of Fig. 11, which individually display a less satisfactory agreement with the Capitelli-Lamanna results.

It is worth noting, however, that this comparison must be considered only under a qualitative point of view. An insight into the Capitelli-Lamanna calculations for $n=2$, in fact, shows that their cross sections have been obtained by a very simple method of calculation and using, in particular, different interaction potentials [7]. On the other hand, however, despite these limitations, the two sets of data seem to be in good agreement, and this can be interpreted as a validation of the present results.

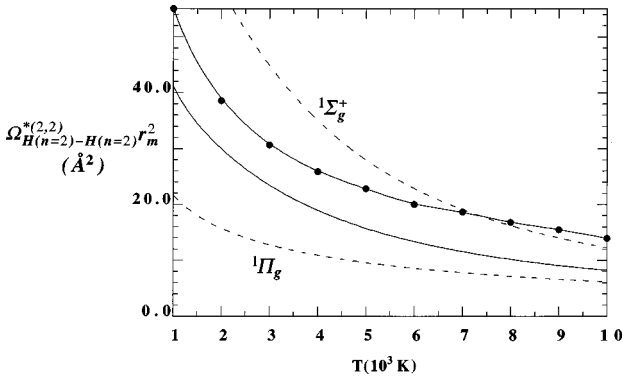


FIG. 11. $\Omega^{*(2,2)}_{\mathrm{H}(n=2)\text{-}\mathrm{H}(n=2)}(T)r_m^2$ as a function of the temperature for H($n=2$)+H($n=2$) scattering system. Dashed lines, collision integrals for $^1\Sigma_g^+$ and $^1\Pi_g$ interactions; solid line, weighted sum (see text); full circles, Capitelli-Lamanna results [3].

### B. Transport coefficients

The viscosity coefficient $\eta$ and thermal conductivity $\lambda$ have been calculated by the usual definitions (first Chapman-Enskog approximation) [14] given as

$$\eta_n(T)=2.6693\times 10^{-5}\,\frac{\sqrt{MT}}{r_m^2\Omega^{*(2,2)}_{\mathrm{H}(n)\text{-}\mathrm{H}(n)}(T)} \tag{16}$$

and

$$\lambda_n(T)=7.4518\,\frac{\eta_n(T)}{M}, \tag{17}$$

where $\eta_n$ is expressed in poise and $\lambda_n$ in cal sec$^{-1}$ cm$^{-1}$ K$^{-1}$, providing that molecular weight $M$ and $r_m^2\Omega^{*(2,2)}_{\mathrm{H}(n)\text{-}\mathrm{H}(n)}(T)$ are given in atomic mass units and in Å$^2$, respectively. For $n=2$, $r_m^2\Omega^{*(2,2)}_{\mathrm{H}(n=2)\text{-}\mathrm{H}(n=2)}(T)$ is the weighted sum of the two contributions coming from the $^1\Sigma_g^+$ and $^1\Pi_g$ states.

In Tables IV and V, the values of viscosity coefficients and thermal conductivities are reported as a function of the temperature for $1\leqslant n\leqslant 5$. The values for $n=1$ have been taken from Ref. [15]. These results show that initially the transport coefficients rapidly decrease as the principal quantum number increases, converging to a limit for higher $n$ values. This behavior is a direct consequence of the enhancement of the transport cross sections with the principal quantum number, which, through Eqs. (14) and (15), causes the increase of the collision integral. This effect can be clearly seen in the simple rigid-sphere model, which assumes the collision integral $\Omega^{*(2,2)}_{\mathrm{H}(n)\text{-}\mathrm{H}(n)}$ to be unity. According to this model, the large dimensions of the excited atoms determine high values of the rigid-sphere cross section $\pi r_m^2$, with the subsequent reduction of the transport coefficients.

The data of Tables IV and V can be used also for future calculations of the transport coefficients for mixtures of H($n$), $H^+$, and $e^-$ to better determine the role of the excited states on the transport properties of plasma systems.

TABLE IV. Viscosity coefficients $\eta$ ($\mu$P) as a function of the absolute temperature for $n=1$ (Ref. [15]) and $n=2,3,4,5$ (present results).

| $T$ (K) | $n=1$ | $n=2$ | $n=3$ | $n=4$ | $n=5$ |
|---|---|---|---|---|---|
| 20 | 7.692 | 0.7350 | 0.4052 | 0.2912 | 0.2609 |
| 30 | 10.10 | 1.019 | 0.5546 | 0.4000 | 0.3586 |
| 40 | 12.57 | 1.290 | 0.6966 | 0.5037 | 0.4520 |
| 50 | 14.90 | 1.551 | 0.8332 | 0.6039 | 0.5422 |
| 60 | 17.06 | 1.803 | 0.9661 | 0.7015 | 0.6303 |
| 70 | 19.07 | 2.049 | 1.096 | 0.7973 | 0.7166 |
| 80 | 20.99 | 2.289 | 1.224 | 0.8915 | 0.8017 |
| 90 | 22.85 | 2.524 | 1.350 | 0.9846 | 0.8857 |
| 100 | 24.67 | 2.754 | 1.474 | 1.077 | 0.9689 |
| 150 | 33.12 | 3.856 | 2.080 | 1.527 | 1.376 |
| 200 | 40.38 | 4.907 | 2.669 | 1.968 | 1.776 |
| 300 | 53.78 | 6.937 | 3.827 | 2.840 | 2.567 |
| 400 | 66.64 | 8.926 | 4.973 | 3.709 | 3.358 |
| 500 | 78.95 | 10.90 | 6.118 | 4.583 | 4.153 |
| 550 | 84.94 | 11.88 | 6.692 | 5.022 | 4.554 |
| 600 | 90.82 | 12.85 | 7.267 | 5.464 | 4.956 |
| 650 | 96.60 | 13.83 | 7.844 | 5.907 | 5.361 |
| 700 | 102.3 | 14.80 | 8.423 | 6.353 | 5.769 |
| 750 | 107.8 | 15.77 | 9.004 | 6.802 | 6.178 |
| 800 | 113.3 | 16.73 | 9.588 | 7.253 | 6.591 |
| 850 | 118.7 | 17.70 | 10.17 | 7.707 | 7.006 |
| 900 | 123.9 | 18.65 | 10.76 | 8.163 | 7.423 |
| 950 | 129.1 | 19.61 | 11.35 | 8.622 | 7.843 |
| 1000 | 134.2 | 20.56 | 11.95 | 9.084 | 8.266 |
| 1500 | 182.0 | 30.05 | 18.03 | 13.85 | 12.64 |
| 2000 | 228.0 | 39.95 | 24.40 | 18.90 | 17.29 |
| 2500 | 274.0 | 50.71 | 31.05 | 24.22 | 22.20 |
| 3000 | 317.0 | 62.53 | 37.99 | 29.81 | 27.36 |
| 4000 | 400.0 | 89.45 | 52.68 | 41.75 | 38.44 |
| 5000 | 481.0 | 120.6 | 68.44 | 54.69 | 50.47 |
| 6000 | 562.0 | 155.5 | 85.22 | 68.59 | 63.42 |
| 7000 | 644.0 | 194.0 | 103.0 | 83.43 | 77.28 |
| 8000 | 727.0 | 235.6 | 121.8 | 99.19 | 92.02 |
| 9000 | 819.0 | 280.1 | 141.5 | 115.8 | 107.6 |
| 10000 | 913.0 | 327.3 | 162.1 | 133.4 | 124.1 |
| 20000 | 2090 | 917.7 | 418.2 | 355.9 | 334.1 |
| 40000 | 5690 | 2596 | 1191 | 1051 | 996.5 |
| 50000 | | 3652 | 1705 | 1523 | 1449 |

## V. COMMENTS

The present calculations completely neglect the role of inelastic channels in the scattering process, i.e., we assume that the inelastic components do not strongly influence the elastic and transport cross sections. To evaluate the importance of these channels in the determination of the cross sections, let us consider the following inelastic processes:

$$\text{(a)}\quad \mathrm{H}(n)+\mathrm{H}(n)\rightarrow \mathrm{H}^{+}+e+\mathrm{H},$$

$$\text{(b)}\quad \mathrm{H}(n)+\mathrm{H}(n)\rightarrow H_2^{+}+e,$$

$$\text{(c)}\quad \mathrm{H}(ns)+\mathrm{H}(ns)\rightarrow \mathrm{H}(np)+\mathrm{H}(np),$$

the last one followed by (rapid) radiative cascade (quenching). The present status of experimental and theoretical cross-section knowledge for these processes is very scanty, but some indirect information will be sufficient to get a general estimate of their importance.

Let us start with the $\mathrm{H}(n=2)+\mathrm{H}(n=2)$ case. The rate coefficient for process (a) has been reported by Dalgarno [16], who gives $\langle \sigma v\rangle \approx 2\times 10^{-8} T^{-1/6}$ cm$^3$ sec$^{-1}$. This value is, for a temperature of 1000 K, about a factor of 20 smaller than the corresponding rate coefficient calculated on the basis of elastic cross sections reported in Fig. 3 for the $\Sigma$ state, and a factor of 4 with respect to the $\Pi$ state of Fig. 5.

Cross sections for process (b) have been experimentaly determined by Brouillard [$\mathrm{D}(2s)+\mathrm{D}(2s)$] in the energy range $10^{-2}-1$ eV [17]. Absolute values decrease with increasing energy from about 100 to 1 Å$^2$, while our elastic cross sections reported in Fig. 3 decrease from 3000 to 1000 Å$^2$ in the same energy range.

TABLE V. Thermal conductivity $\lambda$(mcal/K cm sec) as a function of the absolute temperature for $n=1$ (Ref. [15]) and $n=2,3,4,5$ (present results).

| $T$ (K) | $n=1$ | $n=2$ | $n=3$ | $n=4$ | $n=5$ |
|---|---|---|---|---|---|
| 20 | 0.05690 | 0.005437 | 0.002998 | 0.002154 | 0.001930 |
| 30 | 0.07470 | 0.007540 | 0.004103 | 0.002959 | 0.002653 |
| 40 | 0.09290 | 0.009544 | 0.005153 | 0.003726 | 0.003343 |
| 50 | 0.1100 | 0.01147 | 0.006164 | 0.004467 | 0.004011 |
| 60 | 0.1260 | 0.01334 | 0.007147 | 0.005189 | 0.004662 |
| 70 | 0.1410 | 0.01516 | 0.008108 | 0.005898 | 0.005301 |
| 80 | 0.1550 | 0.01693 | 0.009053 | 0.006595 | 0.005930 |
| 90 | 0.1690 | 0.01867 | 0.009984 | 0.007283 | 0.006552 |
| 100 | 0.1820 | 0.02037 | 0.01090 | 0.007964 | 0.007167 |
| 150 | 0.2450 | 0.02853 | 0.01539 | 0.01130 | 0.01018 |
| 200 | 0.2990 | 0.03630 | 0.01975 | 0.01456 | 0.01314 |
| 300 | 0.3980 | 0.05132 | 0.02831 | 0.02101 | 0.01899 |
| 400 | 0.4930 | 0.06604 | 0.03679 | 0.02744 | 0.02484 |
| 500 | 0.5840 | 0.08062 | 0.04526 | 0.03390 | 0.03072 |
| 550 | 0.6280 | 0.08787 | 0.04950 | 0.03715 | 0.03369 |
| 600 | 0.6720 | 0.09510 | 0.05376 | 0.04042 | 0.03666 |
| 650 | 0.7140 | 0.1023 | 0.05803 | 0.04370 | 0.03966 |
| 700 | 0.7560 | 0.1095 | 0.06231 | 0.04700 | 0.04267 |
| 750 | 0.7970 | 0.1167 | 0.06661 | 0.05032 | 0.04570 |
| 800 | 0.8380 | 0.1238 | 0.07092 | 0.05365 | 0.04875 |
| 850 | 0.8780 | 0.1309 | 0.07526 | 0.05701 | 0.05182 |
| 900 | 0.9160 | 0.1380 | 0.07961 | 0.06038 | 0.05491 |
| 950 | 0.9550 | 0.1451 | 0.08398 | 0.06378 | 0.05802 |
| 1000 | 0.9330 | 0.1521 | 0.08837 | 0.06719 | 0.06115 |
| 1500 | 1.350 | 0.2223 | 0.1334 | 0.1025 | 0.09353 |
| 2000 | 1.700 | 0.2955 | 0.1805 | 0.1398 | 0.1279 |
| 2500 | 2.030 | 0.3752 | 0.2297 | 0.1792 | 0.1642 |
| 3000 | 2.350 | 0.4626 | 0.2810 | 0.2205 | 0.2024 |
| 4000 | 2.970 | 0.6617 | 0.3897 | 0.3088 | 0.2843 |
| 5000 | 3.570 | 0.8920 | 0.5063 | 0.4046 | 0.3733 |
| 6000 | 4.160 | 1.151 | 0.6304 | 0.5074 | 0.4692 |
| 7000 | 4.770 | 1.435 | 0.7619 | 0.6172 | 0.5717 |
| 8000 | 5.380 | 1.743 | 0.9007 | 0.7338 | 0.6807 |
| 9000 | 6.060 | 2.072 | 1.046 | 0.8570 | 0.7961 |
| 10000 | 6.750 | 2.421 | 1.199 | 0.9867 | 0.9178 |
| 20000 | 15.70 | 6.789 | 3.093 | 2.633 | 2.471 |
| 40000 | 43.30 | 19.21 | 8.807 | 7.775 | 7.371 |
| 50000 | | 27.02 | 12.61 | 11.27 | 10.72 |

Quenching cross sections, i.e., the collisional transformation of $H(2s)$ to $H(2p)$ followed by radiative decay, have been determined by Brunetti *et al.* [18]. In particular, these authors have experimentally determined the total cross section (elastic+inelastic) of $H(2s)$ colliding with different partners. Their experimental results were rationalized with a quantum-mechanical calculation showing that the cross section for the inelastic channel is about 1/6 of the elastic one. This point should be taken as an indication of the fact that the hybridization of $2s2p$ orbitals (or equivalently the coupling $\Sigma$-$\Sigma$ states), though important, is, however, negligible compared with the elastic channel. Other transitions between the multiplet manifold could involve $\Sigma$-$\Pi$ rotational coupling, which, however, can be neglected as shown in Ref. [19].

Another inelastic channel could involve the singlet-triplet spin exchange. Calculations reported by Dalgarno [20] also show that these cross sections are small compared with the present elastic cross sections.

All these observations indicate that present elastic cross sections are predominant as compared with inelastic contributions, thus decreasing the importance of a multichannel approach for the calculation of transport cross sections.

In addition, the experimental quenching cross sections for excited atomic hydrogen ($n=3,5$) [21] show that these cross sections decrease with increasing the principal quantum number, thus reinforcing the idea of the predominance of elastic cross sections in the interaction $H(n)+H(n)$ ($n>2$).

## VI. SUMMARY

In this paper we have investigated the dependence of the transport coefficients on the principal quantum number $n$ of two colliding hydrogen atoms. Viscosity and thermal conductivity relative to $H(n)+H(n)$ interactions have been calculated for $2 \leqslant n \leqslant 5$ and compared with the corresponding quantities relative to the ground state of the H atoms.

We have also calculated the diffusion and elastic cross sections and discussed their dependence on the excitation state of the colliding atoms. For the elastic case, we established a simple scaling law able to reproduce with good accuracy the cross-section behavior as a function of the principal quantum number.

Finally, we want to stress that we have acquired useful information on the collisions of two excited hydrogen atoms and, in particular, on the magnitude and behavior of the elastic and transport cross sections. This achievement can help to understand the role that these processes can play in plasma physics. The present calculations can be considered as a first step toward a better characterization of transport coefficients of plasma systems with high concentrations of electronically excited states.

Future improvements of the present calculations can be done by including nonadiabatic transitions through a multichannel approach even though the considerations of Sec. V seem to minimize the role of different inelastic channels in affecting the transport cross sections.

## ACKNOWLEDGMENTS

This work has been partially supported by MURST (under Project No. 9703109065006). The authors thank Professor A. Riera and Dr. R. K. Janev for helpful suggestions on the role of inelastic channels in affecting the present results.

[1] R. K. Janev, *Basic Properties of Fusion Edge Plasmas and Role of Atomic and Molecular Processes*, in *Atomic and Molecular Processes in Fusion Edge Plasmas*, edited by R. K. Janev (Plenum, New York, 1995).

[2] D. R. Schultz, S. Yu. Ovchinnikov, and S. V. Passovets, *Elastic and Related Cross Sections for Low-energy Collisions Among Hydrogen and Helium Ions, Neutral and Isotopes*, in *Atomic and Molecular Processes in Fusion Edge Plasmas*, edited by R. K. Janev (Plenum, New York, 1995).

[3] M. Capitelli and U. T. Lamanna, J. Plasma Phys. **12**, 71 (1974).

[4] M. Capitelli, C. Guidotti, and U. T. Lamanna, J. Phys. B **7**, 1683 (1974).

[5] S. Geltman, *Topics in Atomic Collision Theory* (Academic, New York, 1969).

[6] M. J. Jamieson, A. Dalgarno, and J. N. Yukich, Phys. Rev. A **46**, 6956 (1992).

[7] B. Linder and J. O. Hirschfelder, J. Chem. Phys. **28**, 197 (1958).

[8] M. E. Gersh and R. B. Bernstein, Chem. Phys. Lett. **4**, 221 (1969).

[9] W. Kolos and L. Wolniewicz, J. Chem. Phys. **43**, 2429 (1965).

[10] S. L. Guberman, J. Chem. Phys. **78**, 1404 (1983).

[11] Note that the cross sections for the $X\ ^1\Sigma_g^+$ and $b\ ^3\Sigma_u^+$ interactions, reported in Figs. 4 and 6, respectively, differ from the Gersh and Bernstein results [8] by a factor equal to the statistical weight (1/4 for the singlet and 3/4 for the triplet state) coming from the electronic spin multiplicity.

[12] C. J. Joachain, *Quantum Collision Theory* (North-Holland, Amsterdam, 1975), p. 174.

[13] Hong-sup Hahn, E. A. Mason, and F. J. Smith, Phys. Fluids **14**, 278 (1971).

[14] J. O. Hirschfelder, C. F. Curtiss, and R. B. Bird, *Molecular Theory of Gases and Liquids* (Wiley, New York, 1964).

[15] A. C. Allison and F. J. Smith, At. Data **3**, 317 (1971).

[16] A. Dalgarno, Rev. Mod. Phys. **39**, 850 (1967).

[17] F. Brouillard and X. Urbain, *Rearrangement Processes Involving Hydrogen and Helium Atoms and Ions*, in *Atomic and Molecular Processes in Fusion Edge Plasmas*, edited by R. K. Janev (Plenum, New York, 1995), and private communication.

[18] B. G. Brunetti, S. Falcinelli, E. Giaquinto, A. Sassara, M. Prieto-Manzanares, and F. Vecchiocattivi, Phys. Rev. A **52**, 855 (1995).

[19] C. A. Slocomb, W. H. Miller, and H. F. Schaefer III, J. Chem. Phys. **55**, 926 (1971).

[20] A. Dalgarno, Proc. R. Soc. London, Ser. A **262**, 132 (1961).

[21] J. W. L. Lewis and W. D. Williams, J. Quant. Spectrosc. Radiat. Transf. **16**, 939 (1976).